Diploma Thesis

Study of electron transport in patterned disordered graphene

ELTE

Dániel Nagy

2019

A kutatást a Nemzeti Kutatási Fejlesztési és Innovációs Alap támogatta a Nemzeti Kiválósági Program keretében, a "Kvantumbitek előállítása, megosztása és kvantuminformációs hálózatok fejlesztése" című, 2017-1.2.1-NKP-2017-00001. számú projekt részeként.

ACKNOWLEDGEMENT

I would first like to thank my thesis advisor Dr. László Oroszlány. His door was always open whenever I had any trouble or question about my research.

I would also like to thank the experts who were involved helping me out whenever I needed: Dr. József Cserti, Zoltán Tajkov and Adrián Németh.

Finally, I must express my very profound gratitude to my partner, Nikolett Farkas, to my parents and friends for providing me with unfailing support and continuous encouragement throughout my years of study and through the process of researching and writing this thesis. This accomplishment would not have been possible without them. Thank you.

Dániel Nagy

Contents

Introduction

Graphene is the first experimentally created quasi two dimensional material, and it catalysed a sudden growth in the research of other atomically thin materials [16]. The pure graphene's bandstructure is gapless and half-filled, which makes it a perfect semi-conductor. It's also has peculiar and chemical properties.

Topological insulators are a new, exotic state of matter, which have an insulating band gap in the bulk and possess a robust spin polarised conducting boundary. [9] The origin of these edge states is topological, thus they can not be changed under small perturbation of the system. As a result of these two properties of the edge states, topological insulators are promising candidates in the building of quantum computers and in spintronics. In agreement with the bulk-boundary correspondence. The topological properties of the bulk can be studied via the edge states. Stable topological phases, respecting time reversal symmtery can occur if the spin-orbit coupling is non-negligible.

Despite the promising attributes of pristine graphene, the spin-orbit coupling is very weak, and thus several approaches emerged to enlarge it. Graphene heterostructures and doping with heavy atoms that have strong spin-orbit coupling are two possible ways.

In this thesis we study adatom doped graphene. According to [2] adatoms can partially self-organise themselves through the RKKY interaction, and due to the order a gap opens in the energy spectrum. In [2] the role of spin-orbit coupling was neglected. The aim of the present thesis is to investigate the effect of spin-orbit coupling in a simple model. More precisely we investigated whether the induced gap can be topological. We showed that the system can be both topological and trivial and we deducted the counterintuitive result, that the system can undergo a phase transition in a some range of the parameter space, where the low temperature phase is trivial and the high temperature phase is topological.
The framework of this thesis is based on numerical methods. In the studied systems I determined the size of the band gap through the local density of states and the topological properties were determined through the quantisation of the spin Hall conductivity. The applied numerical method is the kernel polynomial method, which is exceptionally well suited for the calculation of large, non-interacting systems.
In the present work I dedicated the firs chapter to the graphene. In the second and third I introduce the Kekule distortion and the topological insulators, in the fourth I discuss the kernel polynomial method and the last chapter contains my own results.

Chapter 1

Fundamental characteristics graphene

In this chapter I will briefly summarise the basic properties of graphene, it's geometry in real and in reciprocal space, the electronic structure and the low energy effects.

1.1 The geometry of graphene

The graphene is a two dimensional lattice, made up of carbon atoms, which form a honeycomb lattice. The unit cell of graphene consists of 2 atoms and thus we have two sublattices. Let's call the sub-lattices A and B. The carbon-carbon distance is noted as a_{cc} and it is approximately 0.142 nm [1]. The lattice constant $a_l = \sqrt{3}a_{cc}$. Later on I will always express the terms with a_{cc} so I omit the lowercase index. The lattice vectors $\mathbf{a}_1$ and $\mathbf{a}_2$ are set

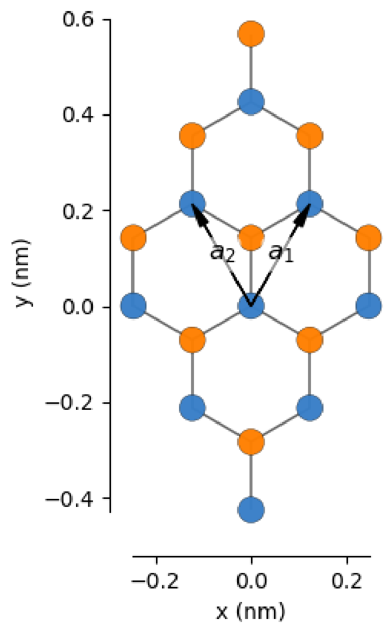

Figure 1.1: graphene, with the lattice vectors $\boldsymbol{a}_1$ and $\boldsymbol{a}_2$. The A and B sublattices have different color.

to:

$$\begin{aligned}
\mathbf{a}_1 =& a\left(\frac{\sqrt{3}}{2}, \frac{3}{2}\right), \\
\mathbf{a}_2 =& a\left(-\frac{\sqrt{3}}{2}, \frac{3}{2}\right).
\end{aligned} \tag{1.1}$$

As we can see in Fig1.1. The Wigner-Zeits cell-size is the length of thre cross-product of the lattice vectors: $\frac{3}{2}\sqrt{3}a_{cc}^2$. The nearest-neighbour (NN) vectors $\boldsymbol{\delta}_i$ are the following:

$$
\begin{aligned}
\boldsymbol{\delta}_1 =& a\left(\sqrt{3}/2, -1/2\right), \\
\boldsymbol{\delta}_2 =& a\left(-\sqrt{3}/2, -1/2\right), \\
\boldsymbol{\delta}_3 =& a\left(0, 1\right).
\end{aligned}
\tag{1.2}
$$

The reciprocal vectors (b_k) are determinedby the orthogonality relation::

$$
\mathbf{a}_k \mathbf{b}_l = 2\pi \boldsymbol{\delta}_{k,l}. \tag{1.3}
$$

yielding:

$$
\begin{aligned}
\mathbf{b}_1 &= \frac{2\pi}{a}\left(\frac{1}{\sqrt{3}}, \frac{1}{3}\right), \\
\mathbf{b}_2 &= \frac{2\pi}{a}\left(-\frac{1}{\sqrt{3}}, \frac{1}{3}\right).
\end{aligned}
\tag{1.4}
$$

1.2 Tight-binding Hamiltonian

In the simplest model we take into consideration the carbon atoms' S_z orbitals with a spin degeneracy of two. The Hamiltonian in second quantized form:

$$
\hat{H} = -t \sum_{\langle i, i+\boldsymbol{\delta} \rangle} (a_i^\dagger b_{i+\boldsymbol{\delta}} + h.c.), \tag{1.5}
$$

where t is the nearest-neighbour hopping with amplitude of 2.8 eV and the i indices label the A sublattice. The annihilation operator a_i annihilates an orbital at site i, $a_i^\dagger$ creates one at site i and h.c. is the Hermitian conjugate. Assuming that the system is periodic, we expand operators "a", "b" and their Hermitian conjugate in Furrier-space to get into the momentum space.

$$
\begin{aligned}
a_m^\dagger &= \frac{1}{\sqrt{N/2}} \sum_{\boldsymbol{k}} e^{i\boldsymbol{k}\boldsymbol{r}_m} a_{\boldsymbol{k}}^\dagger, \\
b_m^\dagger &= \frac{1}{\sqrt{N/2}} \sum_{\boldsymbol{k}} e^{i\boldsymbol{k}\boldsymbol{r}_m} b_{\boldsymbol{k}}^\dagger
\end{aligned}
\tag{1.6}
$$

where we have $\frac{N}{2}$ sites on one sub-lattice. If we plug (1.6) into (1.5) we end up the following:

$$\hat{H} = -t \sum_{\boldsymbol{k}} \left(\sum_{\boldsymbol{\delta}} \mathrm{e}^{-\mathrm{i}\boldsymbol{k}\boldsymbol{\delta}} \right) a_{\boldsymbol{k}}^{\dagger} b_{\boldsymbol{k}} + h.c. \tag{1.7}$$

Introducing $\Psi^{\dagger} = \left(a_{\boldsymbol{k}}^{\dagger}, b_{\boldsymbol{k}}^{\dagger} \right)$ and $\Psi = (a_{\boldsymbol{k}}, b_{\boldsymbol{k}})$ we can recast the Hamiltonian as a 2×2 matrix:

$$H = \sum_{\boldsymbol{k}} \Psi^{\dagger} h(\boldsymbol{k}) \Psi, \tag{1.8}$$

whit $\Delta_{\boldsymbol{k}} = \sum_{\boldsymbol{\delta}} \mathrm{e}^{\mathrm{i}\boldsymbol{k}\boldsymbol{\delta}}$ and the kernel can be written as:

$$h(\boldsymbol{k}) = -t \begin{pmatrix} 0 & \Delta_{\boldsymbol{k}} \\ \Delta_{\boldsymbol{k}}^{*} & 0 \end{pmatrix}. \tag{1.9}$$

1.3 Band structure

The spectrum $E(\boldsymbol{k})$ of the system is obtained by diagonalizing the Hamiltonian (1.9): $E_{\pm}(\boldsymbol{k}) = \pm t \sqrt{\Delta_{\boldsymbol{k}}^{*} \Delta_{\boldsymbol{k}}}$.

So for the of the energy we get:

$$E(\boldsymbol{k}) = t \sqrt{\left(1 + 4 \cos\left(\sqrt{3}/2 \boldsymbol{k}_x a\right) \left[\cos\left(3/2 \boldsymbol{k}_y a\right) + \cos\left(\sqrt{3}/2 \boldsymbol{k}_x a\right)\right]\right)} \tag{1.10}$$

Those $\boldsymbol{k}$ values where (1.10) vanishes define the Dirac-points. If we make a linear approximation around these special points ($E_0(\boldsymbol{k}) \approx 0$) we get the Dirac cones, which are located at the corners of the first Brillouin zone. There are two inequivalent points (**K** and **K**'):

$$K = \frac{2\pi\sqrt{3}}{9a} \left(1, \quad \sqrt{3}\right), \tag{1.11}$$

$$K' = \frac{2\pi\sqrt{3}}{9a} \left(-1, \quad \sqrt{3}\right). \tag{1.12}$$

The calculation of the energy spectra around the **K** point is done by making a first order Taylor-expansion on the energy:

$$E(\boldsymbol{q})_{\pm} = \pm t\partial_{\boldsymbol{k}}|\Delta_{\boldsymbol{k}}|\Big|_{\boldsymbol{k}=\boldsymbol{K}}\boldsymbol{q} \tag{1.13}$$

Where $\boldsymbol{q}$ is in the close vicinity of $\boldsymbol{K}$ ($\boldsymbol{q} = \boldsymbol{\delta k} - \boldsymbol{K}$). In equation (1.13) we expand at first $\Delta_{\boldsymbol{k}}$, which results in:

$$(\partial_{\boldsymbol{k}}\Delta_{\boldsymbol{K}})\boldsymbol{q} \quad = -a\tfrac{3}{2}\mathrm{e}^{-\mathrm{i}\frac{\pi}{3}}(\boldsymbol{q}_{\mathrm{x}} + \mathrm{i}\boldsymbol{q}_{\mathrm{y}}). \tag{1.14}$$

And the energy is given by:

$$E(\boldsymbol{q})_{\pm} = \pm\frac{3}{2}ta|\boldsymbol{q}| \tag{1.15}$$

We could repeat this process, around the $\boldsymbol{K'}$ point as well, and that would yield:

$$(\partial_{\boldsymbol{k}}\Delta_{\boldsymbol{K'}})\boldsymbol{q'} = -a\frac{3}{2}\mathrm{e}^{-\mathrm{i}\frac{\pi}{3}}(-\boldsymbol{q}'_{\mathrm{x}} + \mathrm{i}\boldsymbol{q}'_{\mathrm{y}}) \tag{1.16}$$

from that the energy spectrum also starts linearly:

$$E(\boldsymbol{q}')_{\pm} = \pm\frac{3}{2}ta|\boldsymbol{q}'|. \tag{1.17}$$

We arrived to the conclusion that the energy dependence starts linearly around the Fermi level. We can see the this dependence in the first and second Brillouin zone in Fig.1.2.

The kernel of the Hamiltonian around $\boldsymbol{K}$ is:

$$h(\boldsymbol{q}) = \frac{3}{2}at\begin{pmatrix} 0 & \boldsymbol{q}_x + i\boldsymbol{q}_y \\ \boldsymbol{q}_x - i\boldsymbol{q}_y & 0 \end{pmatrix}. \tag{1.18}$$

Which has a short from:

$$h(\boldsymbol{q}) = \frac{3}{2}at(\boldsymbol{q}_x\boldsymbol{\sigma}^x + \boldsymbol{q}_x\boldsymbol{\sigma}^x) \tag{1.19}$$

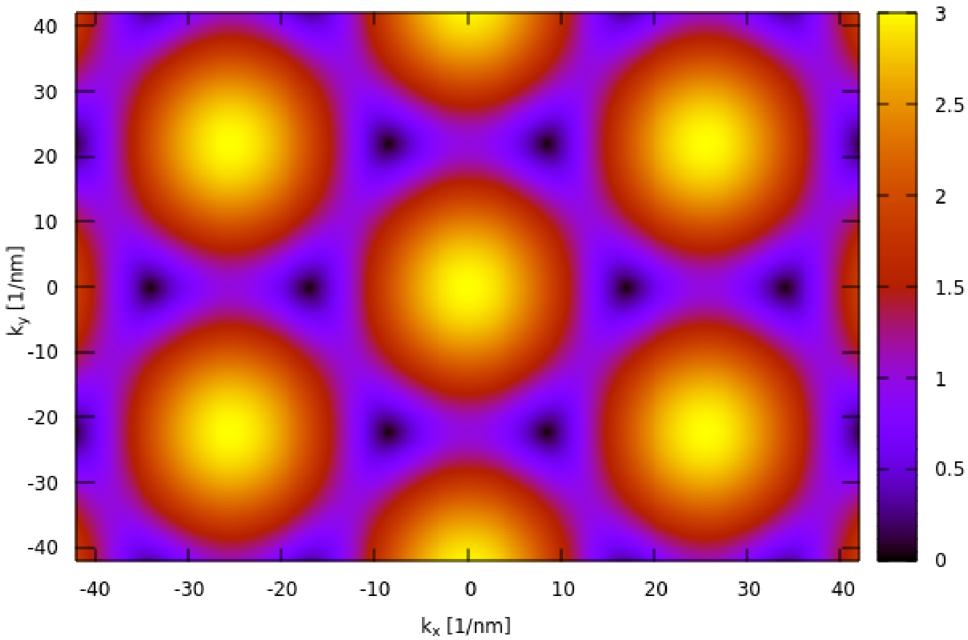

Figure 1.2: A heatmap of the dispersion relation of the conducting band of graphene, showing 6-fold rotational symmetry of the system.

. And near $\boldsymbol{K}'$ it picks up a minus sign:

$$h(\boldsymbol{q}') = \frac{3}{2}at(-\boldsymbol{q}'_x\boldsymbol{\sigma}^x + \boldsymbol{q}'_x\boldsymbol{\sigma}^x) \tag{1.20}$$

.

Chapter 2

Hidden Kekule ordering

Kekule distortion of the honeycomb structure of graphene is an alteration hopping strengths between the NN bonds. In this chapter we explore how Kekule distortion due to adatoms can arise in graphene samples and what are the potentially observable effects.

2.1 Properties of Kekule lattice

Taking a honeycomb superlattice composed by 3 unit cells, where one unit cell is distinguished yields the Kekule lattice see Fig2.1. The NN hoppings are distorted around the substrate (it changes from t to t'). This type of distortion preserves the 6-fold rotational , translational and reflectional symmetries. Due to the peculiar geometry of the attice the K and K' points coincides, which creates an opportunity to benefit from the low-energy intervalley scattering traits. Kekule lattice can be created using an insulating substrate [17]. The Hamiltonian of such systems can be described if we con-

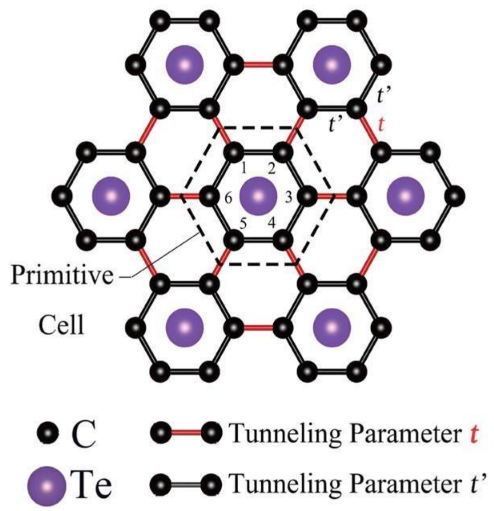

Figure 2.1: Schematic of Kekule distorted lattice [14] caused by Sb_2Te_3 substrate. The two inequivalent hopping parameters are denoted t and t'.

sider the orbitals of the six carbon atom in the unit supercell and view the adatoms via the distortion of t'. This, leads to a periodic system, governed by a 6×6 Hamiltonian, but in low-energies it reduces to a 4×4 effective Hamiltonian around the Dirac-points [4]:

$$\mathrm{H_{ef}} = -\mathrm{u}_{\boldsymbol{q}}^{\dagger} \begin{pmatrix} 0 & h(\boldsymbol{q}) \\ h(\boldsymbol{q}) & 0 \end{pmatrix} \mathrm{u}_{\boldsymbol{q}} \tag{2.1}$$

. Where $u_{\boldsymbol{q}} = (a_{\boldsymbol{k}-\boldsymbol{G}}, a_{\boldsymbol{k}+\boldsymbol{G}}, b_{\boldsymbol{k}-\boldsymbol{G}}, b_{\boldsymbol{k}+\boldsymbol{G}})$ and

$$h(\boldsymbol{q}) = \begin{pmatrix} \frac{3}{2}ta(q_x + iq_y) & 3\frac{1-t'/t}{t} \\ 3\frac{1-t'/t}{t} & \frac{3}{2}ta(-q_x + iq_y) \end{pmatrix} \tag{2.2}$$

Finding the energies corresponding to (2.1) we get a gapped spectrum:

$$\mathrm{E}(\boldsymbol{k}) = \sqrt{(\frac{3}{2}\mathrm{ta})^2 + (3(\mathrm{t} - \mathrm{t}'))^2}, \tag{2.3}$$

which leads to a gapped state if $t \neq t'$.

2.1.1 Adatom induced Kekule ordering

If we want to break the periodicity then we shall use another way of creating Kekule lattice, which is the use of heavy alkali adatoms as doping [2]. The adatoms' energetically favourable position is in the centers of the honeycomb. There are three possible permutation according to the relative position of the adatom. If these relative positions are equivalent we talk about a "one-colored" lattice realisation and if the relative positions differ, then it's a "multi-color" lattice. By sprinkling the doping substances we create a multi-color lattice. By reason of randomness the Hamiltonian takes a little bit different form [2]:

$$H(\boldsymbol{q}) = \frac{3}{2}at\boldsymbol{q}\boldsymbol{\sigma} \otimes \Pi_z + \frac{3}{2}at' \sum_i \boldsymbol{u}_i \boldsymbol{\Pi} \delta(\boldsymbol{r} - \boldsymbol{r}_i) \otimes \sigma_0. \tag{2.4}$$

Where Π acts on the inter-valley, $\boldsymbol{r}_i$ is the position of adatoms and $\boldsymbol{u}_i = (\cos(2\pi/3m_i), \sin(2\pi/3m_i))$ specifies the three different color of adatoms, with $m_i = -1, 0, 1$. According to [6] we find that the RKKY interaction between two adatoms has the form of:

$$V_{i,j} = -J \frac{u_i u_j}{|\boldsymbol{r}_i - \boldsymbol{r}_i|^3}. \tag{2.5}$$

Here J is a positive constant, which contains the electron spin degeneracy. In contrast with the phonon mediated interaction, $V_{i,j}$ has a long-range tail. $V_{i,j}$ depends on the relative position of the adatoms, and this consideration maps the problem to the $S = 1$ three-state Potts model. Respecting the Potts model by renaming the following two lattice states:

- Kekule one color $\rightarrow$ color Potts ferromagnet
- Kekule multicolor $\rightarrow$ color Potts paramagnet.

Investigating V_i, j one can see, that in a color Potts paramagnetic state the energy of the system increases by adding an adatom and in the color Potts ferromagnetic state it decreases. After thermodynamical considerations, if the system's temperature T is $T < T_c$, then the system undergoes a paramagnetic $\rightarrow$ ferromagnetic phase transition [2]. In the ferromagnetic phase (2.4) can be averaged over the positions. If we neglect the contribution of phonons, which is reasonable at low adatom density ρ, the eneregy yields:

$$\mathrm{E}(\boldsymbol{k}) = \sqrt{(\frac{3}{2}\mathrm{ta})^2 + (3(\mathrm{t} - \mathrm{t}')\frac{\rho}{3})^2}. \tag{2.6}$$

Which is the same as (2.3).

Chapter 3

Topological insulators

In this chapter we will review the importance and basic properties of the topological insulators (TI) through two simple models, the Haldane and the Kane-Mele model. To describe the topological invariants we will introduce the concept of Chern number and Z_2 invariant.

3.1 General properties of TI

One of the main goal of condensed matter physics is to categorise the different states of matter. For a long time the categorisation was based on Landau-Ginzburg formalism and spontaneous symmetry breaking. But the discovery of quantum Hall state (QHS) showed, that there are other states that differ in a cardinal way, and the field of topological states of matter emerged. QHS is a 2 dimensional (2D) TI, so it has an insulating bulk and the conducting edge. QHS can only occur when a metal is exposed to a strong external magnetic field. Haldane [8] theorised first that a perfect semiconductor can be in a quantum Hall state without any external magnetic field, if the time reversal (TR) symmetry is broken (e.g. via complex hopping). This state has the name of quantum anomalous Hall state (QAHS). The edge states are chiral because they are one-way charge carriers. C. Kane and E. Male [10] showed that it is possible to have a topological state, while the TR symmetry is preserved. In this case there is a spin filtered charge current at the edges, and they called helical edge states. In general there is a relationship between the system's D dimensional insulating bulk and the D-1 dimensional conducting boundary, which is called bulk-boundary correspondence which guarantees the presence of robust edge states for topologically non trivial bulk systems.

For the qualitative description of TI it is sufficient to use the independent electron approximation, which is presented the previous chapter.

3.2 Symmetries and topological invariants

In this section we will mainly discuss the symmetries of the bulk Hamiltonian and their consequences. Our starting point will be the pristine graphene and its Hamiltonian, which has a form of:

$$\begin{aligned} h(\boldsymbol{k}) &= -t\sum_{i=1}^{3}\begin{pmatrix} 0 & \cos(\boldsymbol{k}\boldsymbol{\delta}_i) + i\sin(\boldsymbol{k}\boldsymbol{\delta}_i) \\ \cos(\boldsymbol{k}\boldsymbol{\delta}_i) + i\sin(\boldsymbol{k}\boldsymbol{\delta}_i) & 0 \end{pmatrix} \\ &= -t\sum_{i}\left[\sigma_x\cos(\boldsymbol{k}\boldsymbol{\delta}_i) + \sigma_y\sin(\boldsymbol{k}\boldsymbol{\delta}_i)\right]. \end{aligned} \tag{3.1}$$

Or around the **K** point:

$$h_0(\boldsymbol{q}) = -t\frac{3}{2}a(\sigma_x\boldsymbol{q}_x + \sigma_y\boldsymbol{q}_y) = \boldsymbol{d}\boldsymbol{\sigma}. \tag{3.2}$$

where $\boldsymbol{\sigma} = (\sigma_x, \sigma_y)$ and $\boldsymbol{d} = -t\frac{3}{2}a(q_x, q_y)$. The Pauli matrices along with the identity ($\mathbb{I}_2$) make a set of basis for 2×2 Hermitian matrices. In an attempt to generalise our model, we introduce the third Pauli matrix, with a coefficient of M. According to (1.8) σ_z introduces an energy difference between the two sublattice and the energy around the Dirac-points becomes gapped:

$$E(\boldsymbol{q})_{\pm} = \pm\sqrt{t^2\Delta^*\Delta + M^2} \tag{3.3}$$

Here 3.3 formally describes massive Fermions, with mass M, and so far as the Hamiltonian doesn't contain any term with proportional with the identity the spectra stays even under $E(\boldsymbol{q}) \rightarrow E(-\boldsymbol{q})$. Now we will go through the symmetries which are relavant for graphene [13]:

- Sublattice (chiral) symmetry, which reads as:

  $$\sigma_z h \sigma_z^{-1} = -h$$

  we get sublattice symmetryif h doesn't contain any terms proportional with σ_z or $\mathbb{I}_2$.

- 3-fold rotational symmetry. This is due to graphene's sp^2 hybridized atomic orbitals, which interchanges the $\boldsymbol{\delta}$-s with each other.

- TR symmetry, which is anti-unitary ($\hat{\mathrm{T}}$). For vectors f it looks like:

  $$\hat{\mathrm{T}}\mathrm{f}(\boldsymbol{r}, \boldsymbol{p}, \boldsymbol{s}) = \mathrm{f}(\boldsymbol{r}, -\boldsymbol{p}, -\boldsymbol{s}) = \mathrm{f}(\boldsymbol{r}, \boldsymbol{p}, \boldsymbol{s}),$$

  where s is the spin. For matrices (rank two operators) it's effect is:

  $$h(\boldsymbol{k}) = h^*(-\boldsymbol{k}).$$

In real space $\hat{\mathrm{T}} = \mathcal{K}$ the complex conjugation: $h(\boldsymbol{r}) = h^*(\boldsymbol{r})$. $\hat{\mathrm{T}}$ operator switches the $\mathbf{K}$ and $\mathbf{K}$' points. It's worth mentioning that if $\boldsymbol{k} = (0,0)$, $\boldsymbol{k} = \pm(\frac{\pi}{a_l}, 0)$ or $\boldsymbol{k} = \pm(0, \frac{\pi}{a_l})$, the $h(\boldsymbol{k}) = h^*(\boldsymbol{k})$ trivially satisfied, since $0 = -0$ and $\frac{\pi}{a_l} = -\frac{\pi}{a_l}$ in the BZ (a_l is the lattice constant).

- Inversion symmetry or parity ($\hat{\mathrm{P}}$):

$$f(\boldsymbol{r}, \boldsymbol{p}, \boldsymbol{s}) = f(\boldsymbol{r}, -\boldsymbol{p}, -\boldsymbol{s})$$
$$h(\boldsymbol{r}) = h(-\boldsymbol{r})$$

In the Haldane model we will break both the TR and sublattice symmetry in order to create a topological phase.

3.3 Haldane model

In the Haldane model we introduce σ_z with a $\boldsymbol{k}$ dependent coefficient. The new Hamiltonian h has the form of

$$h(\boldsymbol{k}) = h_0(\boldsymbol{k}) + M\sigma_z. \tag{3.4}$$

Where M still is to be specified. We want to break the time reversal and the sublattice inversion symmetry, so M should contain an even function of $\boldsymbol{k}$ and it also has a real part, which alone would produce a normal insulator. So far we considered M as a constant. Now we redefine it to $M \to M + 2t_2 \sum_i \sin(\boldsymbol{k}\boldsymbol{b}_i)$. See, how the symmetries are changed due to M:

- m, which breaks the sublattice symmetry. It can be seen as a potential difference between the 2 sublattices and it usually occurs in compounds.

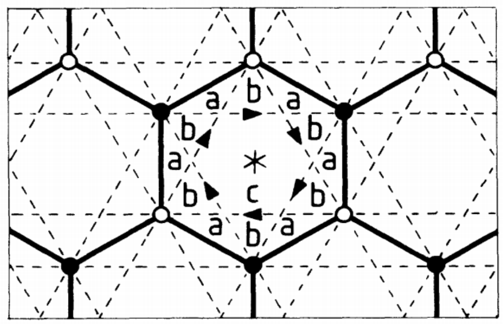

Figure 3.1: Since NNN are complex, there direction is meaningful. By hopping through the following way: $\boldsymbol{b}_1 \rightarrow \boldsymbol{b}_2 \rightarrow \boldsymbol{b}_3$ we make a closed loop. Which can be left or right handed.

- $2t_2 \sum_i \sin(\boldsymbol{k}\boldsymbol{b}_i)$ which breaks both the sub-lattice and the time reversal symmetry. $\boldsymbol{b}_i$ connects the same sub-lattice and the sin function is odd in $\boldsymbol{k}$, hence the symmetry breaking.

The $\boldsymbol{b}_i$ vectors, which connects the A sublattice can be expressed with the $\boldsymbol{\delta}$:

$$\begin{aligned}
\boldsymbol{b}_1 &= \boldsymbol{\delta}_2 - \boldsymbol{\delta}_3 = a(-\frac{\sqrt{3}}{2}, -\frac{3}{2}) \\
\boldsymbol{b}_2 &= \boldsymbol{\delta}_3 - \boldsymbol{\delta}_1 = a(-\frac{\sqrt{3}}{2}, \frac{3}{2}) \\
\boldsymbol{b}_3 &= \boldsymbol{\delta}_1 - \boldsymbol{\delta}_2 = a(\sqrt{3}, 0).
\end{aligned} \tag{3.5}$$

The energy are defined as [8]:

$$E(\boldsymbol{k}) = \sqrt{E_0(\boldsymbol{k})^2 + [m + \sum_i 2t_2 \sin(\boldsymbol{k}\boldsymbol{b}_i)][m + \sum_j 2t_2 \sin(\boldsymbol{k}\boldsymbol{b}_j)]}. \tag{3.6}$$

The relation between the complex NNN hoppings can be seen in Fig.3.1 Now we shall solve the eigenvalue problem of (3.6). And find the gap closings. We already know, that at the $\boldsymbol{K}$ and $\boldsymbol{K}'$ points without the nnn hoppings the energy is zero ($E_0(\boldsymbol{K}) = 0$) and doubly degenerate. If we are neither in the $\boldsymbol{K}$ nor in the $\boldsymbol{K}'$ point the system always will be gapped. So we will investigate around the Dirac-points. The energy simplifies to

$$\begin{aligned} E(\boldsymbol{K})_\pm = \pm|m + \sum_{\boldsymbol{b}} 2t_2 \sin(\boldsymbol{K}\boldsymbol{b})| \\ = \pm|m + 2t_2 3\sin(2\pi/3)| = \pm|m + 2t_2 3\sqrt{3}| \end{aligned} \tag{3.7}$$

and in the $\boldsymbol{K}'$ point:

$$\begin{aligned} E(\boldsymbol{K}')_\pm = \pm|m + \sum_{\boldsymbol{b}} 2t_2 \sin(\boldsymbol{K}'\boldsymbol{b})| \\ = \pm|m + 2t_2 3\sin(-2\pi/3)| = \pm|m - 2t_2 3\sqrt{3}|. \end{aligned} \tag{3.8}$$

If $t_2 = \mp\frac{m}{3\sqrt{3}}$ the gap closes at either the K or K' point. When the spectra is gapped the system is in an insulating state and a gap is closed its in a metallic or semi metallic state.

3.4 Kane-Mele model

A QSH insulator respects time reversal symmetry. Here two edge states with different spin-polarisation propagates opposite directions. So they are called helical edge states. Band crossings are protected by time reversal symmetry. In the Kane-Mele model we make add together (direct sum) 2 Haldane Hamiltonian. One of them is time reversed. The new Hamiltonian reads as:

$$H_{KM} = \begin{pmatrix} H_{TR} & 0 \\ 0 & H_\downarrow \end{pmatrix}. \tag{3.9}$$

Where H_{TR} is the Haldane model's Hamiltonian time reflected version. Here the sum of the 2 Chern numbers vanish, but the difference of them is non-zero, and therefore it can be used to define a new topological number Z_2, that counts the time-reversed pairs of edge modes. If Z_2 is odd then the system is in a topological phase (QSH), otherwise it is a trivial insulator.

Chapter 4

Kernel Polynomial Method

Kernel polynomial method (KPM) is an advanced numerical method, which is useful if one wants to calculate traces of operators which correspond to huge, non-periodic systems. In my thesis I had to numerically evaluate the local density of states and the Hall conductivity for large systems therefore I chose this method. This chapter introduces the basics of this powerful method.

4.1 The Kernel Polynomial Method

Although there are perturbative solutions for disordered systems, but solving them exactly turns out to be nearly impossible. KPM is particularly sufficient numerical method for investigating characteristics of non-interacting systems, or systems describable with sparse matrices, or studying disordered systems. In a D-dimensional Hamiltonian matrix the calculation of all the eigenvalues and eigenfunctions the required memory and time needed scales with D^2 and

D^3 for dense matrices with the use of naive approaches. A handy alternative is the Kernel Polynomial Method (KPM) which uses the Chebyshev expansion to make these calculations possible for large systems. We give up the full and exact knowledge of the spectrum, and instead we approximate the density of states (DOS). The trace of a matrix is basis independent, so we can choose an arbitrary set of basis, when making the evaluation of the conductivity. For that we will use the Chebyshev polynomials and we will introduce a damping kernel to tackle the Gibbs-oscillations. And with an efficient way of approximating the traces of sparse matrices the KPM is viable way of calculating DOS and conductivity of large systems.

4.1.1 Chebyshev polynomials

We use Chebyshev polynomials because they have a uniform convergence on the interval $(-1, 1)$. So in this section I will introduce the properties of these polynomials.

Let's define the scalar product between two integrable functions f and g with a positive weight function $\omega(x)$ as the following:

$$\langle f|g\rangle = \int_{-1}^{1} \omega(x) f(x) g(x) dx. \tag{4.1}$$

With a complete set of orthogonal polynomials $\rho_n(x)$ we can expand any integrable function as

$$f(x) = \sum_{n=1}^{\infty} \alpha_n \rho_n(x), \tag{4.2}$$

where α_n can be determined through the application of the inner product by multiplying (4.2) with $\rho_m(x)$.

$$\alpha_n = \frac{\langle \rho_n(x)|f\rangle}{\rho_n(x)\rho_n(x)}. \tag{4.3}$$

The $\omega(x)$ weight function of the Chebyshev polynomials is $\omega(x) = (\pi\sqrt{1-x^2})^{-1}$ for the T_n first kind and $\omega(x) = \pi\sqrt{1-x^2}$ for the U_n second kind of these polynomials. From the scalar product defined in (4.1) we can get the orthogonality relations as:

$$\langle T_n|T_m\rangle_1 = \tfrac{1+\delta_{n,0}}{2}\delta_{n,m} \tag{4.4}$$

$$\langle U_n|U_m\rangle_2 = \tfrac{\pi^2}{2}\delta_{n,m} \tag{4.5}$$

By substituting $x = \cos\theta$ the Chebyshev polynomials are the unique polynomials satisfying the $T_n(\cos\theta) = \cos(n\theta)$ equation for $n \in \mathbb{N}$ are the first kind, and $U_n(\cos\theta) = \frac{\sin((n+1)\theta)}{sin\theta}$ are the second kind. Now let's recall the even components of the Furrier series:

$$\frac{1}{\pi}\int_0^\pi d\theta \cos(n\theta)\cos(m\theta) = \frac{1+\delta_{n,0}}{2}\delta_{n,m} \tag{4.6}$$

If we write back the $\theta = \arccos x$ expression we get the defining relations:

$$\begin{aligned} T_n(x) &= \cos(n \arccos x) \\ U_n(x) &= \frac{\sin((n+1)\arccos x)}{\sin\arccos x} \end{aligned} \tag{4.7}$$

From the explicit forms we can get the recursion relations by evaluating the first two Chebyshev polynomials (it worth using the $x = \cos\theta$ substitution).

$$
\begin{aligned}
&T_0(\cos\theta) = \cos(0\theta) = 1 \\
&T_1(\cos\theta) = \cos\theta = x \\
&T_n(x) = 2xT_{n-1}(x) - T_{n-2}(x) \\
&U_0(\cos\theta) = \frac{\sin\theta}{sin\theta} = 1 \\
&U_1(\cos\theta) = \frac{\sin(2\theta)}{\sin\theta} = \frac{2\sin\theta\cos\theta}{\sin\theta} = 2x \\
&U_n(x) = 2xU_{n-1}(x) - U_{n-2}(x)
\end{aligned}
\tag{4.8}
$$

We also have a rule for the product of two polynomials of the first kind. We assume that $n \leq m$

$$
2T_m(x)T_n(x) = T_{m+n}(x) + T_{m-n}(x) \tag{4.9}
$$

Which is analogous to the $2\cos(m)\cos(n) = \cos(m+n)+\cos(m-n)$ trigonometric identity.

4.1.2 Modified moments

As we have seen in the previous section a function expanded in terms of the Chebyshev polynomials of the first kind can be written as:

$$
f(x) = \sum_{n=0}^{\infty} \frac{\langle f|T_n\rangle_1}{\langle T_n|T_n\rangle_1} T_n(x) \tag{4.10}
$$

and the coefficient before $T_n(x)$ can be obtained as:

$$
\alpha_n = \frac{\langle f|T_n\rangle_1}{\langle T_n|T_n\rangle_1} = \int_{-1}^{1} dx \frac{f(x)T_n(x)}{\pi\sqrt{1-x^2}}. \tag{4.11}
$$

In practical matrix problems the calculation coefficients defined in (4.11) is cumbersome, so we have to slightly change the expansion, namely:

$$f(x) = \frac{1}{\pi\sqrt{1-x^2}} \left(\mu_0 + 2\sum_{n=0}^{\infty} \mu_n T_n \right), \tag{4.12}$$

where μ_n only differs from α_n in that in the integral the $\omega(x)$ weight function is "missing".

$$\mu_n = \frac{\langle f|\Phi_n\rangle_2}{\langle \Phi_n|T_n\rangle_2} = \int_{-1}^{1} dx f(x) T_n. \tag{4.13}$$

It formally means, that we use the second kind of inner product with the first kind of Chebyshev polynomials :

$$\Phi_n(x) = \frac{T_n(x)}{\pi\sqrt{1-x^2}} \tag{4.14}$$

and $\Phi_n(x)$ satisfies the same orthogonality relations as $T_n(x)$. So the expansion in (4.10) can be rewritten as:

$$f(x) = \sum_{n=0}^{\infty} \frac{\langle f|\Phi_n\rangle_2}{\langle \Phi_n|\Phi_n\rangle_2} \Phi_n(x) = \frac{1}{\pi\sqrt{1-x^2}} \left(\mu_0 + 2\sum_{n=1}^{\infty} \mu_n T_n(x) \right). \tag{4.15}$$

Later on we will discuss on how to regularize the finite order expansions and how to use this numerical method in practice. the modified moments μ_n carry all the information regarding f(x).

4.1.3 Practical considerations

Before using the Chebyshev polynomials we have to rescale the eigenvalues of the considered Hamiltonian into the $(-1, 1)$ interval. To do this we use the power method devised by Lánczos [12]. The rescaled values are:

$$\tilde{H} = \tfrac{H-b}{a} \tag{4.16}$$

$$\tilde{E_n} = \tfrac{E_n-b}{a} \tag{4.17}$$

Where E_n is the n-th eigenvalue of H. Assuming, that all energy lies between $(E_{min}\ ,\ E_{max})$ we get:

$$a = \frac{E_{max} - E_{min}}{2 - \epsilon} \tag{4.18}$$

$$b = \frac{E_{max} + E_{min}}{2} \tag{4.19}$$

where ϵ is a small number, introduced to avoid numerical instability around the border of $(1, -1)$ interval, and a is the scaling factor.

Stochastic evaluation of traces

At first glance we would think that the required time for calculating the traces were proportional to $\mathcal{O}(D^2)$ because the iteration needs to be repeated for all D states of the basis. Luckily, we can obtain a good approximation of the moments with a use of R randomly chosen states $|r\rangle$, where $R \ll D$. The number of R states in some cases can be as low as 1 if we increase D, the size of the system. This can be seen, by considering a set of basis $\{|i\rangle\}$. The we get our states $|r\rangle$ as:

$$|r\rangle = \sum_{i=1}^{D} \zeta_{ri} |i\rangle \tag{4.20}$$

where $\zeta_{ri} \in \mathbb{C}$ are independent, identically distributed random variables and satisfy the following relations in terms of the statistical average:

$$\begin{aligned} \overline{\zeta_{ri}} &= 0 \\ \overline{\zeta_{ri}\zeta_{r\prime j}} &= 0 \\ \overline{\zeta^*_{ri}\zeta_{r\prime j}} &= \delta_{r,r\prime}\delta_{i,j}. \end{aligned} \tag{4.21}$$

Now calculate the average of the trace estimate $\Theta = \frac{1}{R}\sum_{r=1}^{R}\langle r|B|r\rangle$ for an arbitrary chosen B Hermitian operator. The relative error of the estimate trace is $\frac{\delta\Theta}{\Theta}$, the trace of B^2 is usually in the order of $\mathcal{O}(D)$. And the relative error is of order $\mathcal{O}(\frac{1}{\sqrt{RD}})$ [18].

Note, that the distribution of the random variables $\rho(\zeta_{r,i})$ have a slight attribution to the fluctuation. So it is advised to keep $\overline{|\zeta_{r,i}|^4}$ as close to 1 (it's lower bound) as possible. One can achieve this if by choosing $\{\zeta_r, i\}$ to be the uniformly distributed phase of the complex unit. Although this set of random variables are not independent of the basis. So the most natural choice are Gaussian distributed ζ_r, i. In this case $\overline{|\zeta_{r,i}|^4} = 2$, but this is basis independent and so is the $(\delta\Theta)^2$ fluctuation.

When computing local density of states (LDOS), instead of using random vectors, we choose one, or more specific elements of the local basis, with the use of projectors, and we use a vector corresponding to the projected subspace.

Recursive calculation of expectation values

Later on we will use the trace of DOS, LDOS, and the conductivity tensor. We obtain the moments as:

$$\begin{aligned}
\mu_n^D &= \langle\beta|T_n(\tilde{H})|\alpha\rangle \\
\mu_n^L &= \mathrm{Tr}\left(\hat{P}_r T_n(\tilde{H})\right) \\
\mu_{n,m}^\sigma &= \mathrm{Tr}\left(v_x T_n(\tilde{H}) v_y T_m(\tilde{H})\right)
\end{aligned} \tag{4.22}$$

where $|\alpha\rangle$ and $|\beta\rangle$ are states of the system, $\hat{P}_r$ projects to a subspace, corresponding to $\boldsymbol{r}$ and v_x and v_y are the velocity operators' x and y components.

Dealing with μ_n^D is quite straightforward: we create $|\alpha\rangle_n$ from $T_n(\tilde{H})|\alpha\rangle$ and then we make the inner product with $\langle\beta|$. In the construction of $|\alpha_n\rangle$ we use the (4.10) relation:

$$
\begin{aligned}
|\alpha_0\rangle &= |\alpha\rangle \\
|\alpha_1\rangle &= \tilde{H}|\alpha_0\rangle \\
|\alpha_n\rangle &= 2\tilde{H}|\alpha_{n-1}\rangle - |\alpha_{n-2}\rangle
\end{aligned} \tag{4.23}
$$

and the moments:

$$\mu_n^D = \langle\beta|\alpha_n\rangle. \tag{4.24}$$

The calculation of μ_n^L goes quite similarly. By first conducting $< \beta\hat{P}_r| =< \beta|\hat{P}_r|$ the result is:

$$\mu_n^L = \langle\beta\hat{P}_r|\alpha_n\rangle. \tag{4.25}$$

The procedure of receiving $\mu_{n,m}^\sigma$ goes like this: after determining $T_m(\tilde{H})|\alpha >= |\alpha_m >$ we again, make the dot product: $v_y|\alpha_m >= |v_y\alpha_m >$. We get a form similar to the starting point in μ_n^L:

$$\mu_{n,m}^\sigma =< \beta|v_x T_n(\tilde{H})|v_y\alpha_m > . \tag{4.26}$$

The most time consuming part is the multiplication of $\tilde{H}$ to $|\alpha_n\rangle$. If $\tilde{H}$ is a sparse matrix of dimension D then the time needed for a single multiplication is $\mathcal{O}(D)$. And if we want to calculate the first N moments then it will go with $\mathcal{O}(ND)$.

For very large matrices we have to create $\tilde{H}$ on-the-fly in each iteration, but we have to store 2 vectors to create μ_n according to (4.23). And we also eighter need to store $|\beta\rangle$ or we have to create it on-the-fly as well. The overall memory consumption is really low, which allow us to apply this method to large systems.

4.1.4 Kernel polynomials and Gibbs oscillations

Gibbs oscillations

So far we introduced the basics of expanding an integrable function $f(x)$ in an infinite series of Chebyshev polynomials and we know how to calculate the moments μ_n But, since we are discussing a numerical approach we have to truncate the expansion series at some value N. So we are looking for the best (uniform) approximating function $f_{KPM}(x)$. For that reason we will use the concept of kernels, which help to improve the convergence of the mapping from $f(x)$ to $f_{KPM}(x)$. A simple truncation of the expansion would give rise to unwanted oscillations, namely the Gibbs oscillations, near discontinuities or singularities, which leads to poor precision in most physical cases. The function, truncated at the order of N:

$$f(x) \approx \frac{1}{\pi\sqrt{1-x^2}} \left(\mu_0 + 2 \sum_{n=1}^{N-1} \mu_n T_n(x) \right). \tag{4.27}$$

The trick to use damping kernels is that we have to modify the expansion coefficients $\mu_n \to g_n \mu_n$, which depend on N. We get the approximated function as:

$$\begin{aligned} f_{KPM}(x) &= \sum_{n=0}^{N-1} g_n \frac{\langle f|\Phi_n\rangle}{\langle \Phi_n|\Phi_n\rangle} \Phi_n(x) \\ &= \frac{1}{\pi\sqrt{1-x^2}} \left(g_0\mu_0 + 2 \sum_{n=1}^{N-1} g_n \mu_n T_n(x) \right) \end{aligned} \tag{4.28}$$

This method is equivalent of the convolution of $f(x)$ with a kernel form:

$$K_N(x,y) = g_0\Phi_0(x)\Phi_0(y) + \sum_{n=1}^{N-1} g_n\Phi_n(x)\Phi_n(y), \tag{4.29}$$

where $\Phi_n(x)$ are the (4.14) defined polynomials. The estimate function is:

$$f_{KPM}(x) = \langle K_N(x,y)|f(y)\rangle_2 = \int_{-1}^{1} dy\pi\sqrt{1-x^2}K_N(x,y)f(y). \tag{4.30}$$

With this approach the problem translates into finding the optimal kernel, or according to (4.29) finding the appropriate g_n coefficients.

Damping kernels

The Jackson kernel employed in the present work:

$$g_n^J = \frac{(N-n-1)\cos(\frac{\pi}{N+1}n) + \sin(\frac{\pi k}{N+1}n)\cot(\frac{\pi k}{N+1})}{N+1} \tag{4.31}$$

is a the optimal kernel for most applications [18]. The effect of the kernel can be seen in Fig 4.1.

4.1.5 Applications of KPM

Density of states and local density of states

Our first application of the Chebyshev polynomials is the calculation of the spectral density of a D dimensional Hamiltonian:

$$\tilde{\rho}(\tilde{E}) = \frac{1}{D}\sum_{k=0}^{D-1}\delta(\tilde{E}-\tilde{E}_k), \tag{4.32}$$

where the parameters are rescaled so all the eigenvalues $\tilde{E}_k$ of the matrix $\tilde{H}$ lies between the interval $(-1,1)$. We can efficiently calculate the trace using

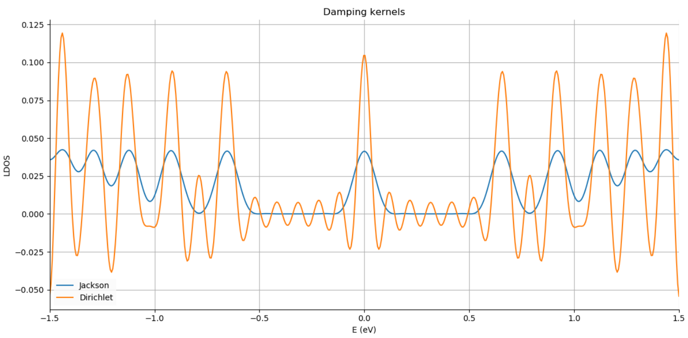

Figure 4.1: Graphene monolayer's local density of states in strong magnetic field. We can see the damping effect of the Jackson kernel. The Dirichlet kernel the trivial kernel.

the stochastic techniques. Using (4.15) we get:

$$\rho(\tilde{E}) = \frac{1}{\pi\sqrt{1-\tilde{E}^2}}[g_0 + 2\sum_{n=1}^{N} g_n Tr(T_n(\tilde{H}))T_n(\tilde{E})]. \tag{4.33}$$

Conductivity

For the dc Kubo conductivity is we have the following formula for noninteracting electrons[11]:

$$\begin{aligned}\sigma_{x,y}(\mu, T) = \frac{ie^2\bar{h}}{\Omega}\int_{-\infty}^{\infty} d\epsilon f(\mu-\epsilon, T)\\ \mathrm{Tr}[\mathrm{v_x}\delta(\epsilon-\mathrm{H})\mathrm{v_y}\frac{\mathrm{dG^+}(\epsilon)}{\mathrm{d}\epsilon} - \mathrm{v_x}\frac{\mathrm{dG^+}(\epsilon)}{\mathrm{d}\epsilon}\mathrm{v_y}\delta(\epsilon-\mathrm{H})].\end{aligned} \tag{4.34}$$

Where Ω is the volume, $f(\mu-\epsilon, T)$ is the Fermi-Dirac distribution, v_x and v_y is the velocity operator and $G^{\pm}$ is retarded/avanged Green function. We can rewrite and rescale G with Chebyshev polynomials according to [5] and [3]:

$$\tilde{G}^{\pm}(\tilde{E}, \tilde{H}) = \mp\frac{i}{\pi\sqrt{1-\tilde{E}^2}}[g_0 + \sum_{n=1}^{N} g_n \mathrm{e}^{\pm \mathrm{in}\arccos(\tilde{\mathrm{E}})}]\mathrm{T_n}(\tilde{\mathrm{H}}). \tag{4.35}$$

With the expressions (4.33) and (4.35) we can calculate expansion of the conductivity tensor. By substituting (4.33) and (4.35) into (4.34) we end up:

$$\sigma_{x,y}(\mu,T) = \frac{16e^2\bar{h}}{\pi\Omega\Delta E^2}\int_{-1}^{1} d\epsilon \frac{f(\mu-\epsilon,T)}{(1-\epsilon^2)^2}\sum_{n,m}\Gamma_{n,m}(\epsilon)g_n g_m \mu^{\sigma}_{n,m}. \tag{4.36}$$

Here $\Delta E = E_{max} - E_{min}$ and the scalar $\Gamma_{n,m}(\epsilon)$ is:

$$\begin{aligned}\Gamma_{n,m}(\epsilon) = (\epsilon - im\sqrt{1-\epsilon^2})\mathrm{e}^{\mathrm{im\,arccos}(\epsilon)}\mathrm{T_n}(\epsilon) - \\ (\epsilon - in\sqrt{1-\epsilon^2})\mathrm{e}^{\mathrm{in\,arccos}(\epsilon)}\mathrm{T_m}(\epsilon)\end{aligned} \tag{4.37}$$

Chapter 5

Spin-orbit coupling induced topological phases in color Potts patterns

In accordance with [2] cooling a Kekule distorted system under the critical temperature T_c there is a phase transition from color Potts paramagnet to color Potts ferromagnet. Further broadening this model by taking into account the spin-orbit coupling topological phase transition becomes possible. My goal was to investigate these phases, and to find out, whether it is possible to induce topological phase transitions with temperature.

5.1 The model

In a Kekule lattice the bulk is always gapped, if the two kind of bonding is different. So gap closings and topological phase transition is impossible.

As we saw earlier, with the introduction of imaginary NNN hoppings we can build a Chern insulator. Thus it is convenient to introduce NNN hopping in a Kekule distorted model. Heavy alkali atoms played the role of doping, so it was convenient to take into account the spin-orbit coupling (SOC). I modelled the influence of adatoms through the perturbation of NN hoppings and the emergence of NNN imaginary hoppings. Two different setup was used: color Potts ferromagnet and color Potts paramagnet. In 5.1 we can see these two different alignment, with different density of disorder (ρ). In topological phase transitions two of the cardinal questions are, with what parameters the gap opens and closes and whether the gapped parts are topological. To answer those questions we will make analytical calculations and perform simulations. Both in the calculation and in the simulation a unit system was used, where the carbon-carbon distance $|\boldsymbol{a}| = 1$ and the pristine graphene's hopping integral $|t| = 1$. The modified NN hoppings are named t' and the imaginary NNN hoppings m.

5.2 Analytical calculation

Only the $\rho = 1/3$ color Potts ferromagnetic system is periodic and for that reason I made the analytical calculation regading only that system.

The supercell arrangement of the supercell can be seen in Fig5.2.

A 6×6 Hermitian matrix is made corresponding to the intracell hoppings. Then we create the transfer matrices T_k using the Bloch-theorem, corresponding to the intercell hoppings. The bulk Hamiltonian has the form

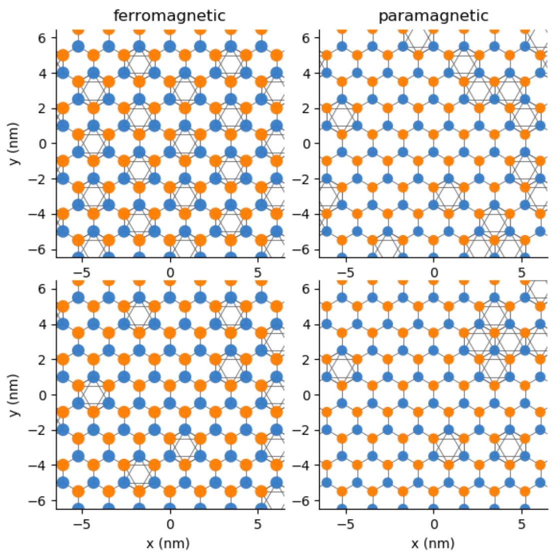

Figure 5.1: Typical impurity patterns for four considered adatom configurations. In the top row a high impurity concentration of $\rho = 1/3$ is depicted for the color Potts ferromagnet and color Potts paramagnet configurations, while in the bottom row a lower concentration of $\rho = 1/6$ is shown. The more ρ decreases the less the difference between the two adatom configuration is visible, even though their electronic properties might be characterised by different topological phases.

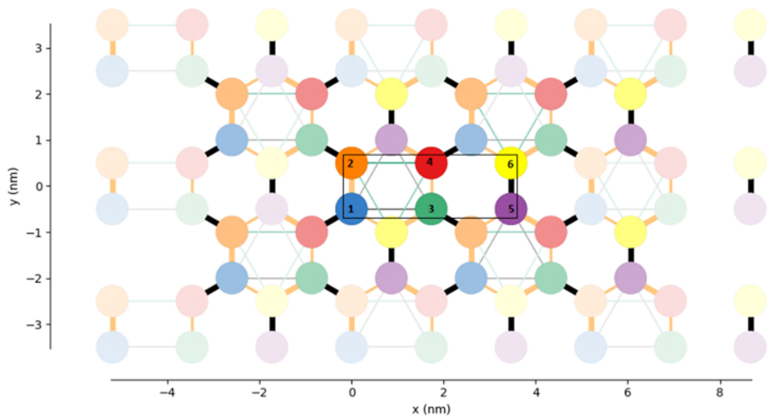

Figure 5.2: The rectangle shows the super unit cell.

of:

$$\hat{H}^{Sup}(\boldsymbol{k}) = U + \left[T_1 \mathrm{e}^{\mathrm{i}\boldsymbol{k}(\boldsymbol{A}_1 - \boldsymbol{A}_2)} + \mathrm{T}_2 \mathrm{e}^{\mathrm{i}\boldsymbol{k}\boldsymbol{A}_2} + \mathrm{h.c.}\right]. \tag{5.1}$$

Where

$$\begin{aligned} \boldsymbol{A}_1 &= (3\sqrt{3}a_{cc}, 0) \\ \boldsymbol{A}_2 &= (\frac{3\sqrt{3}a_{cc}}{2}, \frac{3a_{cc}}{2}) \end{aligned} \tag{5.2}$$

$$U = \begin{bmatrix} 0 & t' & im & 0 & 0 & 0 \\ t' & 0 & 0 & -im & 0 & 0 \\ -im & 0 & 0 & t' & 0 & 0 \\ 0 & im & t' & 0 & 0 & 0 \\ 0 & 0 & 0 & 0 & 0 & t \\ 0 & 0 & 0 & 0 & t & 0 \end{bmatrix}$$

$$T_1 = \begin{bmatrix} 0 & 0 & 0 & 0 & 0 & 0 \\ 0 & 0 & 0 & 0 & 0 & 0 \\ 0 & t & 0 & 0 & 0 & 0 \\ 0 & 0 & 0 & 0 & 0 & 0 \\ im & t' & -im & t' & 0 & 0 \\ 0 & 0 & 0 & 0 & 0 & 0 \end{bmatrix} T_2 = \begin{bmatrix} 0 & 0 & 0 & t & 0 & t' \\ 0 & 0 & 0 & 0 & 0 & im \\ 0 & 0 & 0 & 0 & 0 & t' \\ 0 & 0 & 0 & 0 & 0 & -im \\ 0 & 0 & 0 & 0 & 0 & 0 \\ 0 & 0 & 0 & 0 & 0 & 0 \end{bmatrix}$$

Considering the fact that the Dirac-points are folded back to the Γ-point and we are look for the low energy solution we can substitute $\boldsymbol{k} = 0$ into (5.1). And setting $t = -1$ the Hamiltonian simplifies to:

$$H^{Sup} = \begin{bmatrix} 0 & t' & im & -1 & -im & t' \\ t' & 0 & -1 & -im & t' & im \\ -im & -1 & 0 & t' & im & t' \\ -1 & im & t' & 0 & t' & -im \\ im & t' & -im & t' & 0 & -1 \\ t' & -im & t' & im & -1 & 0 \end{bmatrix} \tag{5.3}$$

The zero-energy modes of (5.3) can be obtained by demanding $\det(\mathrm{H}^{\mathrm{Sup}}) = 0$.

The solutions are the following:

$$\begin{aligned} t' &= \frac{1}{2} \\ m &= \pm\frac{\sqrt{3}}{3}|t'+1| \end{aligned}. \tag{5.4}$$

We keep only the physically relevant solution: where $t' < 0$. Since the whole model is TR invariant both m and $-m$ occur, but with different spin polarization. This calculation main purpose is to check if the simulation is working well.

5.3 Numerical evaluations

For the lattice creation and the Hamiltonian building the pybinding [15] scientific package was used and for the numerical evaluation the Kwant package [7]. I made and run the simulations on my computer. I worked in a lattice with a total number of lattice sites $N \approx 1.3 \times 10^5$. I made a code, which measures the size of the gap: if the absolute value of the energy is smaller than a predefined energy threshold ($E_{th} = 10^{-3}$ eV) it is considered as zero. E_{th} is in a good agreement of the lattice size and the energy resolution, and varying it by a small amount does not change the energy band gap size. The following simulations were done on both the color Potts ferromagnetic and color Potts paramagnetic cases:

- parameter space mapping
- Kubo-conductivity.

In the parameter space mapping I calculated the local density of states (LDOS) on 6 randomly chosen lattice sites. On the parameter space the NN bond strength t' and the NNN bond strength m was varied in the intervals $[-2.5, 0]$ and $[0, 0.5]$ in a 40×40 meshgrid. I made these LDOS calculations for adatom density $\rho = 1/3$ and $\rho = 1/6$.

The quantum Hall conductivity, being a topological characterisation of the system, can not be changed in a connected gapped region. And knowing that, the length of the plateau is equal to the size of the band gap, so for the better numerical results I chose the parameters m and t' where the gap was maximal. I averaged over the result 100 conductivity calculation.

At those chosen parameters m and t' the LDOS is also plotted alongside with the conductivity.

5.3.1 Color Potts ferromagnet

Although there are three separate sector in this case in the parameter space mapping, there are only two topologically distinct cases: when $m < \sqrt{3}/3t'$ it is in a topologically trivial state, with a corresponding zero cross-conductivity, and when $m > \sqrt{3}/3t'$ it's in a TI phase. When $\rho = 1/3$ and $\rho = 1/6$ we can see the the conductivity in Fig5.3 and in Fig5.4, where we can see that the analytical calculation have a good agreement with the numerical evaluations. It's notable that as we lower ρ the band gap size decreases, and the evaluations become less accurate.

5.3.2 Color Potts paramagnet

In the color Potts paramagnetic phase there is only one gapped region. And it's topological phase was determined by calculating the spin Hall conductivity. It is in a topological phase as we can see it in Fig 5.5 for $\rho = 1/3$ and

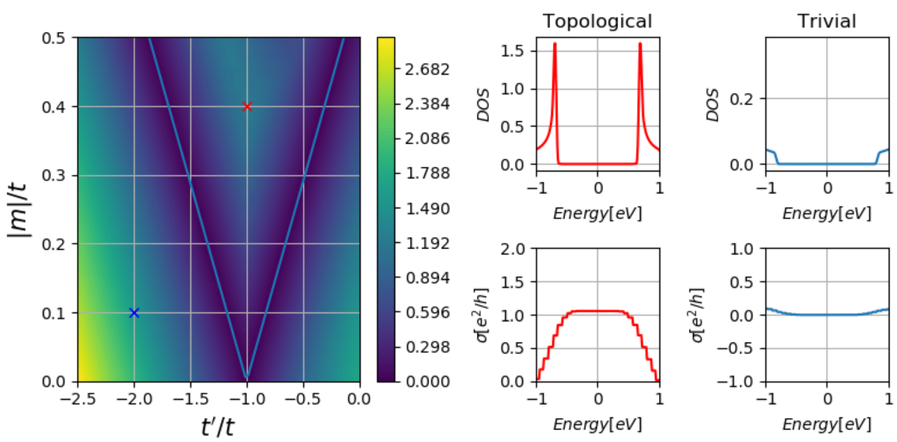

Figure 5.3: Color ferromagnetic lattice configuration, with $\rho = 1/3$. The colormap shows the size of the gap corresponding to the hopping terms. The 'x'-es mark the values of the parameters, where the conductivities were calculated. The blue line corresponds to the analytical calculation. On the right side we can see the spin Hall conductivity on the bottom row and the corresponding LDOS on the upper row.

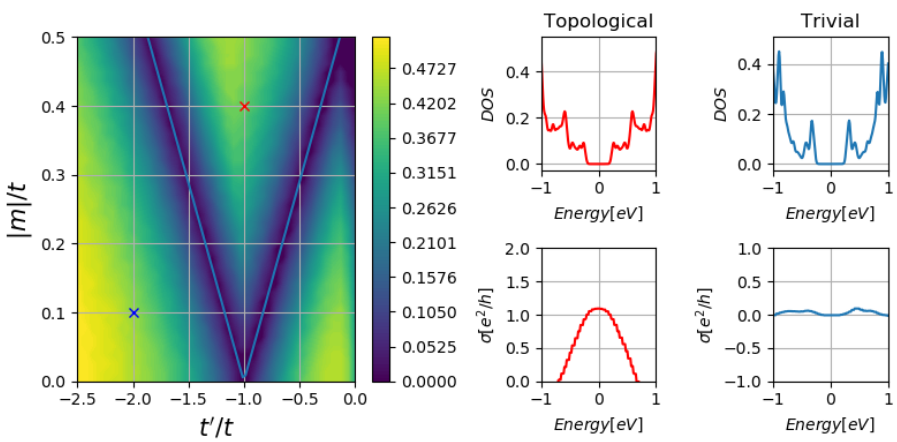

Figure 5.4: Color ferromagnetic lattice configuration, with $\rho = 1/6$. The colormap shows the size of the gap corresponding to the hopping terms. The 'x'-es mark the values of the parameters, where the conductivities were calculated. The blue line corresponds to the analytical calculation. On the right side we can see the spin Hall conductivity on the bottom row and the corresponding LDOS on the upper row.

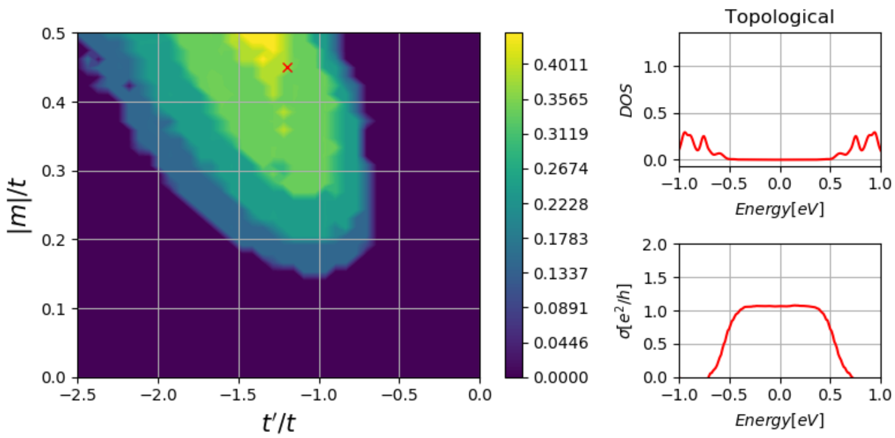

Figure 5.5: Color paramagnetic lattice configuration, with $\rho = 1/3$. The colormap shows the size of the gap corresponding to the hopping terms. The 'x' marks the values of the parameters, where the conductivity was calculated. On the upper right side we can see the Hall conductivity and on the bottom right the corresponding LDOS.

for $\rho = 1/6$ in Fig5.6.

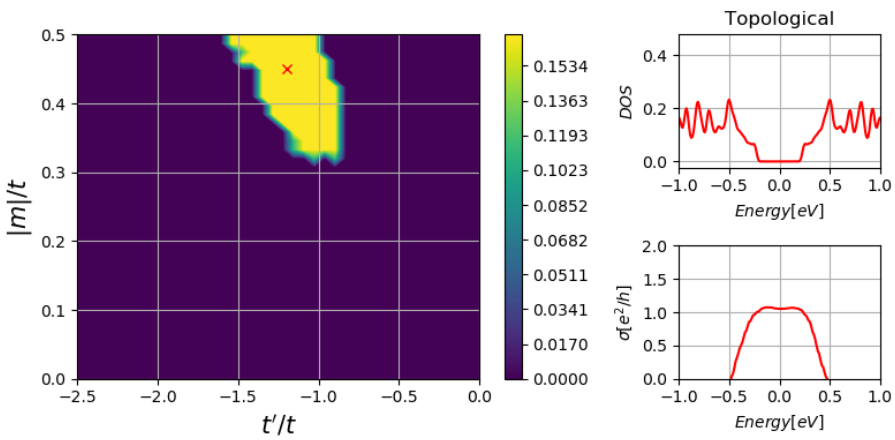

Figure 5.6: Color paramagnetic lattice configuration, with $\rho = 1/6$. The colormap shows the size of the gap corresponding to the hopping terms. The 'x' marks the values of the parameters, where the conductivity was calculated. On the upper right side we can see the Hall conductivity and on the bottom right the corresponding LDOS.

Discussion

In this thesis I studied the topological nature of the quasiparticle gap in adatom doped graphene. With the help of numerical methods and the calculation of both density of states and conductivity the topological phases were characterised. According to an earlier study [2] adatoms on low temperature tend to partially self-organisation, which leads to a topologically trivial band gap. High temperature destroys the order and closes the gap. In this work I showed that by considering the adatom induced spin-orbit coupling the consequences about the forbidden gap significantly changes: while in the low temperature regime the system can be either in trivial or in topological insulating phase depending on the parameters, in high temperature if the system displays any gap, then it must be topological. Consequently, in a certain range of paramters in the studied systems there is a finite temperature phase transition, where the low temperature phase corresponds to the trivial phase and the high temperature to the topological phase.
In this work I only studied the extremely low temperature, fully color ordered phase and the extreme high temperature adatom patterns. Thus a natural extension of this study would be to consider partial color ordering and explore evolution of the system as temperature is changed.

Bibliography

[1] A. H. Castro Neto, F. Guinea, N. M. R. Peres, K. S. Novoselov, and A. K. Geim. “The electronic properties of graphene”. In: *Rev. Mod. Phys.* 81 (1 Jan. 2009), pp. 109–162.

[2] V.V. Cheianov, V.I. Fal’ko, O. Syljuåsen, and B.L. Altshuler. “Hidden Kekulé ordering of adatoms on graphene”. In: *Solid State Communications* 149.37 (2009), pp. 1499–1501. ISSN: 0038-1098.

[3] Aires Ferreira and Eduardo R. Mucciolo. “Critical Delocalization of Chiral Zero Energy Modes in Graphene”. In: *Phys. Rev. Lett.* 115 (10 Aug. 2015), p. 106601.

[4] O V Gamayun, V P Ostroukh, N V Gnezdilov, İ Adagideli, and C W J Beenakker. “Valley-momentum locking in a graphene superlattice with Y-shaped Kekulé bond texture”. In: *New Journal of Physics* 20.2 (Feb. 2018), p. 023016.

[5] Jose H. Garcia, Lucian Covaci, and Tatiana G. Rappoport. “Real-Space Calculation of the Conductivity Tensor for Disordered Topological Matter”. In: *Phys. Rev. Lett.* 114 (11 Mar. 2015), p. 116602.

[6] L. González-Árraga, F. Guinea, and P. San-Jose. “Modulation of Kekulé adatom ordering due to strain in graphene”. In: *Phys. Rev. B* 97 (16 Apr. 2018), p. 165430.

[7] Christoph W Groth, Michael Wimmer, Anton R Akhmerov, and Xavier Waintal. “Kwant: a software package for quantum transport”. In: *New Journal of Physics* 16.6 (June 2014), p. 063065. URL: `https://doi.org/10.1088%2F1367-2630%2F16%2F6%2F063065`.

[8] F. D. M. Haldane. “Model for a Quantum Hall Effect without Landau Levels: Condensed-Matter Realization of the ”Parity Anomaly””. In: *Phys. Rev. Lett.* 61 (18 Oct. 1988), pp. 2015–2018.

[9] M. Z. Hasan and C. L. Kane. “Colloquium: Topological insulators”. In: *Rev. Mod. Phys.* 82 (4 Nov. 2010), pp. 3045–3067.

[10] C. L. Kane and E. J. Mele. “Z_2 Topological Order and the Quantum Spin Hall Effect”. In: *Phys. Rev. Lett.* 95 (14 Sept. 2005), p. 146802.

[11] Ryogo Kubo. “Statistical-Mechanical Theory of Irreversible Processes. I. General Theory and Simple Applications to Magnetic and Conduction Problems”. In: *Journal of the Physical Society of Japan* 12.6 (1957), pp. 570–586. eprint: `https://doi.org/10.1143/JPSJ.12.570`.

[12] C Lanczos. “An iteration method for the solution of the eigenvalue problem of linear differential and integral operators,” in: *NISTJournalofResearch; NISTresearchlibrary; fedlink* (1950).

[13] Sir Anthony Leggett. *Selected Topics in Condensed Matter Physics: A Quantum Information Perspective.* 2010.

[14] Zhuonan Lin, Wei Qin, Jiang Zeng, Wei Chen, Ping Cui, Jun-Hyung Cho, Zhenhua Qiao, and Zhenyu Zhang. "Competing Gap Opening Mechanisms of Monolayer Graphene and Graphene Nanoribbons on Strong Topological Insulators". In: *Nano Letters* 17.7 (2017). PMID: 28534404, pp. 4013–4018. eprint: `https://doi.org/10.1021/acs.nanolett.6b05354`.

[15] Dean Moldovan, Misa Andelkovic, and Francois Peeters. *pybinding v0.9.4: a Python package for tight- binding calculations.* July 2017. URL: `https://doi.org/10.5281/zenodo.826942`.

[16] K. S. Novoselov, A. K. Geim, S. V. Morozov, D. Jiang, Y. Zhang, S. V. Dubonos, I. V. Grigorieva, and A. A. Firsov. "Electric Field Effect in Atomically Thin Carbon Films". In: *Science* 306.5696 (2004), pp. 666–669. ISSN: 0036-8075. eprint: `https://science.sciencemag.org/content/306/5696/666.full.pdf`.

[17] Abhay Shukla, Rakesh Kumar, Javed Mazher, and Adrian Balan. "Graphene made easy: High quality, large-area samples". In: *Solid State Communications* 149.17 (2009), pp. 718–721. ISSN: 0038-1098.

[18] Alexander Weiße, Gerhard Wellein, Andreas Alvermann, and Holger Fehske. "The kernel polynomial method". In: *Rev. Mod. Phys.* 78 (1 Mar. 2006), pp. 275–306.